COMPONENT PART NOTICE

THIS PAPER IS A COMPONENT PART OF THE FOLLOWING COMPILATION REPORT:

(TITLE): Proceedings of the Conference on Improvement of Aerodynamic Performance through Boundary Layer Control and High Lift Systems Held at the Fluid Dynamics Panel Symposium in Brussels, Belgium on 21 23 May 1984.

(SOURCE): Advisory Group for Aerospace Research and Development, Neuilly-sur-Seine (France).

TO ORDER THE COMPLETE COMPILATION REPORT USE AD A147 396.

THE COMPONENT PART IS PROVIDED HERE TO ALLOW USERS ACCESS TO INDIVIDUALLY AUTHORED SECTIONS OF PROCEEDINGS, ANNALS, SYMPOSIA, ETC. HOWEVER, THE COMPONENT SHOULD BE CONSIDERED WITHIN THE CONTEXT OF THE OVERALL COMPILATION REPORT AND NOT AS A STAND-ALONE TECHNICAL REPORT.

THE FOLLOWING COMPONENT PART NUMBERS COMPRISE THE COMPILATION REPORT:

COMPONENT PART NOTICE (CON'T)

AD#:		TITLE:
	P004 069	Pneumatic Turbulators - A Device for Drag Reduction at Reynolds Numbers below 5, 000, 000.
	P004 070	Active and Passive Shock/Boundary Layer Interaction Control on Supercritical Airfoils.
	P004 071	Transonic Shock Interaction with a Tangentially-Injected Turbulent Boundary Layer.

PNEUMATIC TURBULATORS - A DEVICE FOR DRAG REDUCTION AT REYNOLDS NUMBERS BELOW 5 $\times 10^6$

K.H. Horstmann
A. Quast
Institut für Entwurfsaerodynamik der DFVLR
3300 Braunschweig, Germany

L.M.M. Boermans
Delft University of Technology
Dept. of Aerospace Eng.
NL 2629 HS Delft, Netherlands

SUMMARY

At Reynolds numbers below 5 million, airfoils are affected by laminar separation bubbles which, in many cases, considerably increase the drag. By blowing air from a row of orifices at the beginning of the laminar separation bubble, the bubble can be prevented and the drag can be reduced substantially. This device is called pneumatic turbulator. Free-stream total pressure is sufficient to provide the turbulator bleed air. The additional drag caused by the bleed air and the air jets is negligible. The low drag Reynolds number range of laminar airfoils can be extended by using pneumatic turbulators.

SYMBOLS

c_ℓ		Lift coefficient
c_f'		Local friction coefficient
c_p		Pressure coefficient
c_Q		Turbulator bleed air coefficient $c_Q = \frac{\dot{V}}{U_\infty \cdot S}$
c_d		Airfoil section drag coefficient
dc_d		Drag component of the additional pressure Δc_p due to a laminar separation bubble
H		Shape factor $H = \frac{\delta^*}{\theta}$
c	m	Airfoil chord
Re		$\frac{U_\infty \cdot c}{\nu}$ Reynolds number based on airfoil chord c
Re_{δ^*}		$\frac{U_x \cdot \delta^*}{\nu}$ Reynolds number based on displacement thickness δ^*
Re_θ		$\frac{U_x \cdot \theta}{\nu}$ Reynolds number based on momentum loss thickness θ
S	m^2	Wing area
u'	m/s	Longitudinal velocity fluctuation
U		Velocity in the viscous shear layer
U_p		(Hypothetical) inviscid flow velocity
U_{po}		Hypothetical inviscid flow velocity at the surface
U_x	m/s	Local velocity calculated from local static pressure
U_∞	m/s	Free-stream flow velocity
$\dot{V}$	m^3/s	Volumetric flow of air jets
x	m	Chordwise distance
x_T	m	Turbulator position
y	m	Distance from the surface
y_o	m	Distance where U = 0; reversed flow region
α	deg.	Angle of attack
γ	deg.	Slope angle of airfoil contour
δ^*	m	Displacement thickness $\delta^* = \int \left(\frac{U_p}{U_{p0}} - \frac{U}{U_{p0}} \right) dy$
Δc_p		Differential pressure coefficient
Δc_d		Additional drag
η_K	deg.	Flap angle
θ		Momentum loss thickness $\theta = \int \frac{U}{U_{p0}} \left(\frac{U_p}{U_{p0}} - \frac{U}{U_{p0}} \right) dy$
ν	m^2/s	Kinematic viscosity

Subscript

TE	Trailing edge

1. INTRODUCTION

At Reynolds numbers below about five million, laminar separation bubbles can occur on wings and fuselages. These bubbles are generated by a laminar separation of the flow followed by transition and turbulent reattachment. Laminar separation bubbles are undesirable because they increase the drag by mechanisms which have not yet been fully understood.

The following paper describes the details of laminar separation bubbles and provides a hypothesis of the drag mechanism. Furthermore a device called pneumatic turbulator is presented by which laminar separation bubbles can be avoided, thus leading to a drag reduction. Experimental results on laminar airfoils show the effectiveness of this new device, also in comparison with mechanical turbulators. The application range of the pneumatic turbulators is given.

2. DESCRIPTION OF LAMINAR SEPARATION BUBBLES

Laminar separation bubbles occur, if the laminar boundary layer separates from the surface. Due to the destabilizing effect of the boundary layer velocity profiles with an inflection point the laminar boundary layer rapidly becomes unstable and transition occurs in the free shear layer. Next the turbulent boundary layer reattaches, thus forming a bubble as indicated in figure 1. Figure 1 also shows a typical pressure distribution caused by such a bubble in contrast to a pressure distribution (dashed line) without a separation bubble. The laminar part of the bubble is characterized by nearly constant pressure and the turbulent part by a very steep pressure rise. Due to the change in effective airfoil contour, the pressure in front of and behind the bubble is affected too.

Figure 2 shows a schematic drawing of an oil flow pattern which is frequently observed if the airfoil is vertically mounted in the windtunnel, along with a hypothesis of the internal flow in the bubble. The gradient of the oil flow is an indication of the shear stress: nearly horizontal flow is related to a high shear stress and vertical flow is due to gravity and zero shear.

In the front part of the oil flow pattern the oil flow lines become steeper and finally merge into a vertical line representing the separation line.

In the laminar part of the bubble the oil indicates a slowly moving flow in reversed direction near the surface. The turbulent part of the bubble is indicated by reversed oil flow with high shear stress. In between these rotating flows probably a contrarotating vortex is present. At reattachment there is a fir-tree like flow pattern which is governed by stagnation line flow and shear stress.

It should be mentioned that the oil flow pattern at the end of the bubble frequently indicates a three-dimensional flow character, probably due to three-dimensional waves (originating from the unstable Tollmien-Schlichting waves) or Taylor-Goertler vortices. Accordingly, the drag distribution measured with a wake rake traversing along the model span shows a wavy character.

The size of the laminar separation bubble is related to the stability of the laminar boundary layer which in turn depends on Reynolds number and velocity gradient. By increasing the Reynolds number transition is moving forward and the size of the bubble decreases as shown by the measurements on airfoil HQ 17/14.38 in figure 3. At $Re = 2.5 \cdot 10^6$ there seems to be no bubble anymore. Behind decelerated laminar flow the bubble will be short or non-existent and behind accelerated flow the bubble will be longer. Hence, the bubble dimensions vary with angle of attack, as shown in figure 3 too. It is noted that also in case of transition without a bubble ($\alpha = 4.2^\circ$, $x/c = 0.55$, upper surface), a hump is present in the pressure distribution caused by the change in boundary layer displacement thickness and hence in the effective airfoil contour.

Going into more detail, figure 4 shows results of hot-wire anemometer measurements at several stations on the lower surface of the airfoil. The velocity profiles, longitudinal turbulence intensity profiles (u'), and turbulent frequency spectra (not shown here) were measured perpendicular to the airfoil surface. First the results obtained with the clean surface (continuous line) will be considered. The results obtained with turbulators (broken line) will be discussed in the next chapter.

A laminar separation bubble is present on the lower surface between $x/c = 0.73$ where laminar separation takes place, and $x/c = 0.81$ where the boundary layer reattaches. Since the hot-wire cannot detect the direction of the flow, the velocities in the lower region of the bubble are misleading. Just behind reattachment, at $x/c = 0.82$, the velocity profile shows a characteristic dint which disappears rapidly downstream as the boundary layer develops into its fully turbulent state. Outside this turbulent boundary layer the velocity shows a slight gradient due to curvature of the flow. Linear extrapolation provides the hypothetical inviscid velocity at the surface U_{po}, which is used as reference in the velocity and turbulence intensity profiles.

Frequency spectra indicate that in the laminar boundary layer several frequencies are amplified, but the turbulence intensity remains very low. In the free shear layer of the bubble, however, the turbulence intensity, in particular the amplitude at 425 Hz, significantly grows. Just in front of $x/c = 0.80$ the pressure distribution shows a sharp corner, generally considered as the position of transition. In the subsequent steep pressure rise both the size of the turbulent region and the intensity of the turbulent motion

drastically grow, as indicated by the profiles at x/c = 0.8 and x/c = 0.82. Frequency spectra show the amplified 425 Hz frequency and its harmonics to be present in the outer flow up to several boundary layer thicknesses from the surface! Hence, the turbulence intensity is not zero at the edge of the boundary layer. Downstream of reattachment the velocity and turbulence intensity near the surface rapidly increase, suggesting a boundary layer velocity profile at reattachment similar to separation, and a large increase of the shear stress thereafter. Downstream of x/c = 0.84 the turbulence intensity decreases, being distributed in the growing boundary layer thickness, and frequency spectra show a regular pattern without peaks. Outside the boundary layer the amplified 425 Hz frequency is present, its power decreases with distance from the surface.

3. ADDITIONAL DRAG OF LAMINAR SEPARATION BUBBLES

It is well-known that laminar separation bubbles can cause additional drag. This additional drag is composed of additional pressure drag and frictional drag on different parts of the surface. Because of the difficulties in calculating the contribution of the pressure drag current profile drag prediction methods compute profile drag by calculating for each surface the development of the momentum loss thickness θ and applying the well-known Squire-Young relation

$$c_d = 2 \frac{\theta_{TE}}{c} \left(\frac{U_{TE}}{U_\infty} \right)^{\frac{H_{TE}+5}{2}}$$

in order to correct the momentum defect at the trailing edge (TE) to conditions far downstream. Both pressure drag and frictional drag are incorporated this way.

Following this approach the development of the boundary layer parameters calculated from previous velocity profiles (figure 4) is shown in figure 5. Again, first the results plotted by a continous line will be considered.

Due to the weak pressure gradient the laminar boundary layer development approximates the flat plate case, where H = 2.6. As mentioned earlier, the velocity profiles in the reversed flow region of the laminar separation bubble are misleading. Noting that the velocities in that region are very low, one can write

$$\delta^* = \int_0^\infty \left(1 - \frac{U}{U_x}\right) dy = y_o + \int_{y_o}^\infty \left(1 - \frac{U}{U_x}\right) dy$$

$$\theta = \int_0^\infty \frac{U}{U_x}\left(1 - \frac{U}{U_x}\right) dy = \int_{y_o}^\infty \frac{U}{U_x}\left(1 - \frac{U}{U_x}\right) dy$$

which indicates that the reversed flow mainly contributes to the value of δ^*. The increase of δ^* up to the position of transition, and subsequent reduction is evident in figure 5. Contrary, the reattaching and turbulent mixing process involves a sharp increase in momentum loss thickness. Consequently, the shape factor increases to an extremely large value and steeply decreases thereafter. Further downstream a fully turbulent boundary layer develops.

When the boundary layer is artificially disturbed in the vicinity of the laminar separation position, the bubble can be avoided. Figure 4 also shows the pressure distribution and boundary layer profiles measured with a transition strip at x/c = 0.72 (broken line). The strip consists of self-sticking Mylar-film (width 11 mm, thickness 0.25 mm) with digged-in bumps of 1 mm height every 5 mm. Experiments showed that the height of the bumps is just sufficient to trigger the boundary layer.

Behind the strip, at x/c = 0.74, the velocity profile is only slightly affected, however the strip provides turbulence with a primary frequency component of 3600 Hz. Further downstream the boundary layer is much thinner than in the bubble case and the turbulence is concentrated within the boundary layer; the frequency spectra show a regular pattern without peaks.

The corresponding boundary layer parameters in figure 5 also indicate a fully turbulent boundary layer some distance behind the strip.

Applying the Squire-Young relation to the local values of the momentum loss thickness, shape factor and velocity give the development of the equivalent drag values along the surface; the resulting figure is similar to the development of momentum loss thickness. The extrapolated values at the trailing edge indicate that elimination of the bubble reduces the drag contribution of the lower surface by 25% which corresponds to the measured reduction in airfoil drag of 13%.

From these considerations the following tentative conclusions are drawn, illustrated by the schematic sketch in figure 6. In case of a pronounced laminar separation bubble ①,

indicated by the magnitude of the pressure jump for the reattaching transitional shear layer to overcome the increase in momentum loss thickness in this region is the main reason for the drag increase. Triggering the boundary layer in the vicinity of the laminar separation position may easily result in a drag decrease ③ . However, if the bubble is thin or small triggering may be ineffective or even harmful ② . An example of the latter case is given in reference [1].

With respect to profile drag prediction methods, it is clear that the flow mechanism at the rear of the bubble, which define the starting conditions of the turbulent boundary layer, play a crucial role. No method is known to the authors which handles this satisfactorily. As a consequence, drag prediction in case of laminar separation bubbles is not very reliable yet.

Finally, it is noted that there is a lower limit of the Reynolds number Re_θ based on the momentum loss thickness below which no turbulent boundary layer flow can exist. For instance, Preston shows that this Reynolds number for a flat plate at zero pressure gradient is 320, reference [2], and that in case of lower values, the drag of the transition device should increase Re_θ up to this value.

As mentioned in the beginning of this chapter, the additional drag due to a bubble is composed of additional pressure drag and frictional drag.

While the frictional drag contribution of the turbulent boundary layer can be measured for instance by a pitot-probe (Preston-tube), measurements inside the bubble are difficult. A pitot-probe gives a wrong indication when the flow direction exeeds ±30 degrees and hot wire probes generally do not indicate the flow direction. Probably laser velocimetry will give the answers.

With respect to pressure drag, the next considerations clarify some typical features. Figure 7 shows again the change in pressure distribution due to a bubble, and the resulting additional pressure drag component which can be written as

$$\Delta c_d = \int \Delta c_p \cdot \sin(\gamma + \alpha) d(x/c) \ .$$

$(\gamma + \alpha)$ is the angle of the surface with respect to the oncoming flow. If this angle is zero ($\alpha = -\gamma$), there is no additional pressure drag. Compared to the lift of the airfoil section, the additional lift component is negligible.

The following numerical values illustrate the pressure drag contribution due to a bubble. Assuming that there is no bubble anymore on the lower surface at $Re = 2.5 \cdot 10^6$, the measured pressure distributions of figure 3 can be integrated according to the previous equation, taking

$$\Delta c_p = c_{p\ Re} - c_{p(Re=2.5\cdot10^6)}.$$

The pressure drag values listed in table 1 are of the same order of magnitude as the drag reductions caused by pneumatic turbulators*), indicating that the frictional drag contribution due to the bubble is relatively low. A comparison is given in table 1. The results should be considered with care because integration could only be performed approximately since there were only 5 pressure holes in the region of the laminar separation bubble being not sufficient for an accurate representation of the pressure distribution.

The effect of laminar separation bubbles on the drag polars is shown schematically in figure 8. Figure 8a represents the effect of a laminar separation bubble on the upper surface of an airfoil. A characteristic feature is the increase of the additional drag with increasing lift coefficient (angle of attack), which is in accordance with the previous equation. Another characteristic feature is the reduction of drag at the upper limit of the laminar bucket. This reduction is due to the disappearance of the laminar separation bubble since, at higher angles of attack, suction peaks form at the leading edge and the subsequent pressure rise destabilizes the boundary layer in such a way that a normal laminar-turbulent transition occurs prior to laminar separation.

Figure 8b shows the inverse behaviour due to the additional drag of an airfoil with a lower side bubble. The polar of an airfoil with a bubble on upper and lower side would be as shown in figure 8c. The hatched area indicates the additional drag caused by bubbles on upper and lower surface.

Figure 9 shows a practical example of such a drag polar. The airfoil is the Wortmann FX 66-S-196V1 and the measurements were taken from reference [3]. The drag reduction at the limits of the low drag bucket due to the disappearance of the bubble on either surface is obvious, indicating that an elimination of the bubble on both surfaces by triggering would result in a drag reduction between zero lift and nearly maximum lift.

4. DRAG REDUCTION BY MEANS OF PNEUMATIC TURBULATORS

4.1 Description of bubble avoiding devices

As clarified in the previous chapter, laminar separation bubbles are responsible for

*) pneumatic turbulators are discussed in detail in chapter 4.2

the increased drag of some airfoil sections. To prevent these laminar separation bubbles, different techniques can be used. One of these techniques first used by Wortmann [4] is to shape the airfoil sections with so-called destabilizing regions as shown in figure 10. Destabilizing regions are parts of the airfoil with a slightly adverse pressure gradient which promotes transition without laminar separation. At optimum design of the destabilizing region transition occurs just at the end of the region.

Destabilizing regions, however have the following disadvantages:

- A destabilizing region can only be correct for one particular Reynolds number. As indicated in figure 11, at lower Reynolds numbers a separation bubble forms as a result of insufficient destabilization whilst at higher Reynolds numbers the laminar-turbulent transition occurs too early because of too much destabilization. In both cases, drag is higher than necessary.

- A destabilizing region can only be correct for one particular angle of attack or flap angle. With a higher angle of attack, for instance, the pressure increase is steeper on the upper side and flatter on the lower side.

As a result we can notice, that for an airfoil with only one design point there is no need for turbulators; an optimum design can be performed using only destabilizing regions. As far as there is more than one design point with respect to angle of attack, flap deflection and Reynolds number turbulators are an additional powerful tool to avoid drag originating from laminar separation bubbles.

Other devices are mechanical turbulators consisting of trip wires, steps, artificial roughness of sand grains or wire brackets bonded to the skin. D. Althaus has shown that small strips of tape and tape with digged-in bumps prevent the occurence of laminar separation bubbles [5,6]. Experiments performed by Henningsen [7] showed that porous surfaces covering aluminium honeycomb also acted as "turbulators". With a smooth porous panel, transition from laminar to turbulent flow occured considerably further forward than with a non-porous panel. It was not possible to achieve the original aim of damping out Tollmien-Schlichting oscillations; in the contrary, it appeared that the transition from laminar to turbulent flow was even promoted by the porous surfaces.

4.2 Description of pneumatic turbulators

A transition from laminar to turbulent flow is easily achieved using air jets because the laminar flow is disturbed in three dimensions, thus producing the transition very rapidly. If turbulators are not needed, the air jets can simply be switched off. Experimental techniques frequently make use of these jets of air ejected from a series of holes near the leading edge of an airfoil in order to achieve premature transition from laminar to turbulent flow [8]. In doing this, the aim is to simulate the flow conditions at high Reynolds numbers. Wallis [9] has used air jets practically as a substitute for normal "vortex generators" (but switchable) in order to prevent early turbulent separation. Pfenninger [10] has used rows of air jets in order to prevent laminar trailing edge separation.

In order to prevent laminar separation bubbles, the air jets should operate in the vicinity of the separation line as shown in references [11] and [12]. The jets of air are produced by small tubes with an internal diameter of 0.6 mm which are spaced in spanwise direction at intervals of 1.6 ÷ 3.2% of the wing chord. The air for the jets is supplied by an internal duct with total pressure which if necessary can be reduced by suitable devices, thereby reducing the volume of air emerging from the jet orifices.

Pneumatic turbulators offer the further advantage that they are still active in the region behind laminar separation. A mechanical turbulator submerged within the separated region of the bubble is ineffective. A jet of air, on the other hand, passes through this region and disturbs the laminar flow outside the bubble. This is an important point since the turbulators should remain effective even in the area of the laminar separation bubble (i.e. behind the point of laminar separation) because the bubble can move due to Reynolds number, angle of attack and flap deflection.

In principle, it should be possible to achieve similar results by sucking as well as blowing air through orifices, since a sink in the flow also represents a three-dimensional disturbance. However, there are currently no experimental results available on this subject.

4.3 Results for different airfoils

The effect of pneumatic turbulators can be seen in figure 12, showing the characteristics of airfoil DU-80-176, measured in the windtunnel of the Delft University of Technology. Oil-flow patterns indicated the existence of pronounced laminar separation bubbles downstream of the pressure rise at $x/c \approx 0.65$. The air volume flow for the turbulators was adjusted to practical sailplane application: an intake nozzle was dimensioned such that the turbulators worked well at practical combinations of lift coefficient and Reynolds number.

A slightly more cambered version of this airfoil was applied in modifying the wing of an existing high performance sailplane just by adding material to the surface. Flight performance measurements before and after the wing modification showed an improvement of about

5% in glide ratio over the entire flight speed range [13].

Another example which illustrates the effectiveness of pneumatic turbulators is given in figure 13, showing drag and pressure distribution for the airfoil DFVLR-HQ-26/14.82 measured in free flight on the flying testbed sailplane "JANUS" of DFVLR Braunschweig. Turbulators are located at x/c = 0.892 on the lower surface. Again, the drag is reduced by the turbulators. According to chapter 3 the drag reduction decreases with increasing lift coefficient. The pressure distribution without a separation bubble is represented by the dashed line obtained by using pneumatic turbulators. Without these turbulators there is the characteristic pressure increase in front of laminar separation and the pressure flattening thereafter as shown in figure 1. The characteristic steep pressure rise at the rear part of the bubble is missing because it is located behind the trailing edge.

Figure 14 shows results of free flight and windtunnel measurements on the same model with airfoil HQ-17/14.38, mentioned before. The flap was set at $\eta_K = -8°$ and measurements were performed without turbulators, with mechanical turbulators (tape with bums) and with pneumatic turbulators at two different Reynolds numbers. A remarkable drag reduction by turbulators can be seen and furthermore this figure shows that mechanical turbulators nearly have the same effectiveness in this case as pneumatic turbulators.

As in figure 12, in the "no turbulacor case" there is a drag reduction at the lower limit of the laminar drag bucket due to the disappearance of the bubble on the lower surface as a result of destabilization of the flow behind a leading edge pressure peak.

The influence of pneumatic turbulators on drag in the Reynolds number region of model airplane is shcwn in figure 15. The measurements are taken in the small cascade windtunnel of DFVLR Braunschweig [14]. The turbulators are arranged on the upper surface of the airfoil DFVLR-RA-02/K at x/c = 0.445. The drag reduction due to turbulators is strongly increasing with decreasing Reynolds number. A maximum drag reduction of about 40% can be obtained at $Re = 0.1 \cdot 10^6$. At lift coefficients $c_L > 0.8$ the polars with and without turbulators have nearly the same development. In this region the instabilization of the boundary layer is high enough to cause transition upstream of the separation point and thus no bubble is present. It is remarkable that pneumatic turbulators do not cause additional drag, when transition occurs upstream of the turbulator position and hence the turbulators disturb the turbulent boundary layer.

4.4 Parameter investigations

As mentioned before, the size of laminar separation bubbles increase with decreasing Reynolds number. Hence, the drag reduction by turbulators increase too, as shown in figure 16.

In figure 17 the effect of turbulators position on drag reduction at the same airfoil as in figure 15 is shown. There exists an optimum turbulator position close to the laminar separation point. If the turbulators are arranged upstream of the optimum position the drag coefficient increases due to the smaller region of laminar flow. At downstream positions the drag coefficient increases too, due to remaining parts of the bubble between and before the turbulators bleed holes.

The optimum turbulator position is slightly depending on the Reynolds number. With lower Reynolds number the optimum position as well as the laminar separation point is moving upstream. Especially at very low Reynolds number this effect can be seen clearly because the larger laminar separation bubbles (40% of chord at $Re = 0.1 \cdot 10^6$) are more influencing the pressure distribution upstream of the bubble than a smaller one thus inducing a more upstream occuring separation.

Figure 18 shows a typical example of the drag curve with air jet coefficient c_Q (or air volume flow per pneumatic turbulator). As the air volume flow increases, the drag drops initially due to a shrinking of the laminar separation bubble. Next the drag remains at a low level, hardly affected by the amount of air blowing out of the turbulators.

The energy loss (additional drag) as a result of the ram air diverted to the air jets amounts to

$$\Delta c_d = 2\, c_Q \ .$$

Since the drag coefficient of a laminar airfoil is of the order of 5.10^{-3} this additional drag, being in the order of $5 \cdot 10^{-6}$, is negligible.

As shown in figure 18, a certain minimum amount of air is needed for the pneumatic turbulators to function well. Similarly, a certain minimum height of the mechanical turbulators is needed to trigger the boundary layer. An example of malfunction of mechanical turbulators is shown in figure 19. The airfoil and test techniques are the same as in figure 14, but now the flap is set at $\eta_K = -12°$. At both Reynolds numbers the mechanical turbulators (tape with digged-in bumps, about 0.1% c high and 5% c spacing) do their job if positioned at 72% chord on the lower surface. Due to the flap deflection the pressure distribution changes such that the flow should be triggered just in front of the flap, at 80% chord. As shown, an extra drag reduction of about 10% is obtained at $Re = 3 \cdot 10^6$, however there is a turbulator malfunction at $Re = 1.55 \cdot 10^6$ and c_L below 0.45. Turbulator malfunction of this type was up to now never observed with pneumatic turbulators.

5. THE RANGE OF APPLICATION FOR PNEUMATIC TURBULATORS

It has been shown that pneumatic turbulators prevent laminar separation bubbles and thus extend the low-drag Reynolds number range of airfoil sections.

Pneumatic turbulators can be applied successfully if:

- laminar separation bubbles occur and
- an airfoil section is required with a wide operating range as far as the Reynolds number, lift coefficient and flap deflection are concerned.

There would thus appear to be the following potential applications:

1. cascades in turbomachinery
2. propellers and helicopter rotors
3. gliders and light aircraft
4. RPV and model aircraft.

Experiments with turbine cascades at low Reynolds numbers with different transition devices, conducted at the main cascade test facility in Braunschweig, showed that especially pneumatic turbulators reduce the drag of cascade arrangements in a wide range of Reynolds numbers. Air jets on the suction side were supplied through holes from the pressure side.

6. CONCLUSIONS

At Reynolds numbers below 5 million and if a wide range of operation concerning lift coefficient, flap deflection and Reynolds number is demanded, it is advantageous to implement turbulators in laminar airfoil design. Careful positioning of turbulators near the laminar separation point avoids laminar separation bubbles and reduces the drag. Turbulators enlarge the low drag Reynolds number range of an airfoil giving nearly the same drag which is otherwise obtained by several airfoils designed for minimum drag at different Reynolds numbers.

Therefore the design philosophy for airfoils with turbulators differs considerably from that used up to date in laminar airfoil design: the design of airfoils with turbulators should be based on the maximum Reynolds number for the range of the airfoil and not on average Reynolds number.

Besides well-known mechanical turbulators consisting of bump tape pneumatic turbulators were introduced. Pneumatic turbulators consist of air jets expelled from a row of orifices positioned in spanwise direction close to the laminar separation line simply supplied by total pressure. The energy loss (additional drag) of the air jets is negligible compared to the drag reduction due to the very low air volume flow.

Experimental results of four different airfoils for sailplane and model airplane application taken in windtunnel and free flight tests show that the pneumatic turbulators are very effective, reducing the airfoil drag in the order of 40% at $Re = 0.1 \cdot 10^6$ and 15% at $Re = 1 \cdot 10^6$.

Mechanical turbulators in general give the same results in drag reduction. But they should be used carefully because their height has to be adapted to the flow conditions. Otherwise they may be submerged into the separated flow of the bubble and becoming ineffective.

A very interesting further application of pneumatic turbulator would appear in turbine cascades.

7. REFERENCES

[1] Boermans, L.M.M. Oolbekkink, B. Windtunnel Tests on an Outer Wing Segment of the ASW-19X Sailplane.
Report LR-369 (1983), Delft University of Technology, Dept. of Aerospace Engineering.

[2] Preston, J.H. The Minimum Reynolds Number for a Turbulent Boundary Layer and the Selection of a Transition Device.
Journal of Fluid Mechanics, Vol. 3 (1957), pp. 373-384.

[3] Gooden, J.H.M. Experimental Low-Speed Aerodynamic Characteristics of the Wortmann FX66-S-196V1 Airfoil.
Ostiv Publication XV, 1980.

[4] Wortmann, F.X. — Experimentelle Untersuchungen an neuen Laminarprofilen für Segelflugzeuge und Hubschrauber.
Z. Flugwiss. 5 (1957), H. 8, pp. 228-243.

[5] Althaus, D. — Profilpolaren für den Modellflug.
Neckar-Verlag, Villingen-Schwenningen, 1980.

[6] Althaus, D. — Influencing Transition on Airfoils.
XVII. OSTIV Congress, Paderborn, Germany, 1981.

[7] Henningsen, A.W. — Versuche zur Dämpfung von Grenzschichtschwingungen mittels poröser Oberfläche.
Studienarbeit DFVLR Braunschweig, Prof. Dr.-Ing. F. Thomas, Januar 1979.

[8] Ashill, P.R. Weeks, D.J. — An Experimental Investigation of the Drag of Thick Supercritical Aerofoils - A Progress Report.
Lecture Transonic Configuration Symposium, Bad Harzburg, Germany, 13-17 June, 1978.

[9] Wallis, R.A. — The Use of Air Jets for Boundary Layer-Control.
ARL (Australia) Aero. Note 110 (1952).

[10] Pfenninger, W. — Untersuchungen über Reibungsverminderungen an Tragflügeln, insbesondere mit Hilfe von Grenzschichtabsaugung.
Mitt. a.d. Inst. f. Aerodynamik, ETH Zürich Nr. 13, Verlag Gebr. Leeman & Co., Zürich, 1946.

[11] Horstmann, K.H. Quast, A. — Widerstandsverminderung durch Blasturbulatoren.
DFVLR-FB 81-33 (1981).

[12] Quast, A. Horstmann, K.H. — Anordnung zur Beeinflussung der Strömung an aerodynamischen Profilen.
Deutsche Patentanmeldung P 30 43 567.7.-53.

[13] Boermans, L.M.M. Selen, H.J.W. — Design and Tests of Airfoils for Sailplanes with an Application to the ASW-19B.
ICAS-Paper 82-5.5.2, Seattle, USA, 1982.

[14] Voth, M.-A. — Experimentelle Untersuchungen an einem Tragflügelprofil im Reynoldszahlbereich von $1.0 - 2.0 \cdot 10^5$.
Studienarbeit DFVLR Braunschweig, Prof. Dr.-Ing. F. Thomas, 1983.

Re	$\Delta c_d = \Delta c_p \cdot \sin(\gamma + \alpha)\, d(x/c)$	Drag reduction measured as a result of pneumatic turbulators
$0.7 \cdot 10^6$	0.0025	0.0027
$1.0 \cdot 10^6$	0.0019	0.0018
$1.5 \cdot 10^6$	0.0011	0.0012
$2.0 \cdot 10^6$	0	0.0006

Table 1 Comparison of the calculated pressure drag Δc_d of the separation bubble with the measured drag reduction with pneumatic turbulators used on the lower side of airfoil section HQ-17/14.38, $\eta_K = -10^o$, $\alpha = 5^o$.

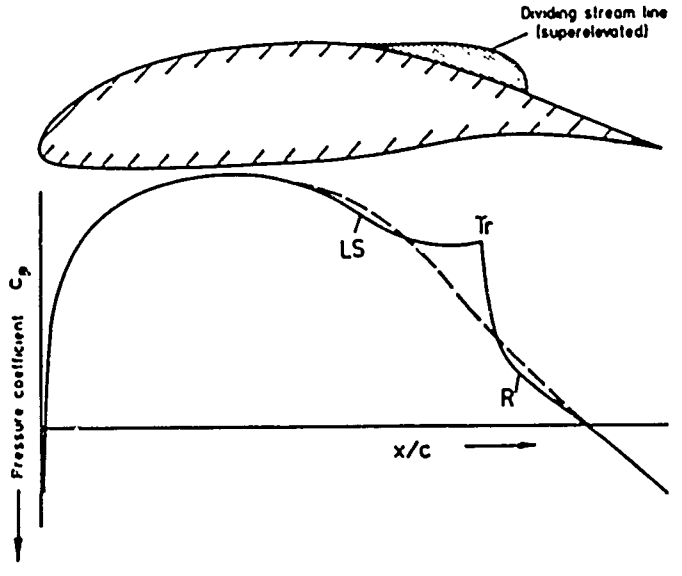

Fig. 1 Characteristic pressure distribution of the upper surface of an airfoil section with laminar separation bubble and assumed dividing streamline
LS = Laminar separation; Tr = Transition;
R = Reattachment

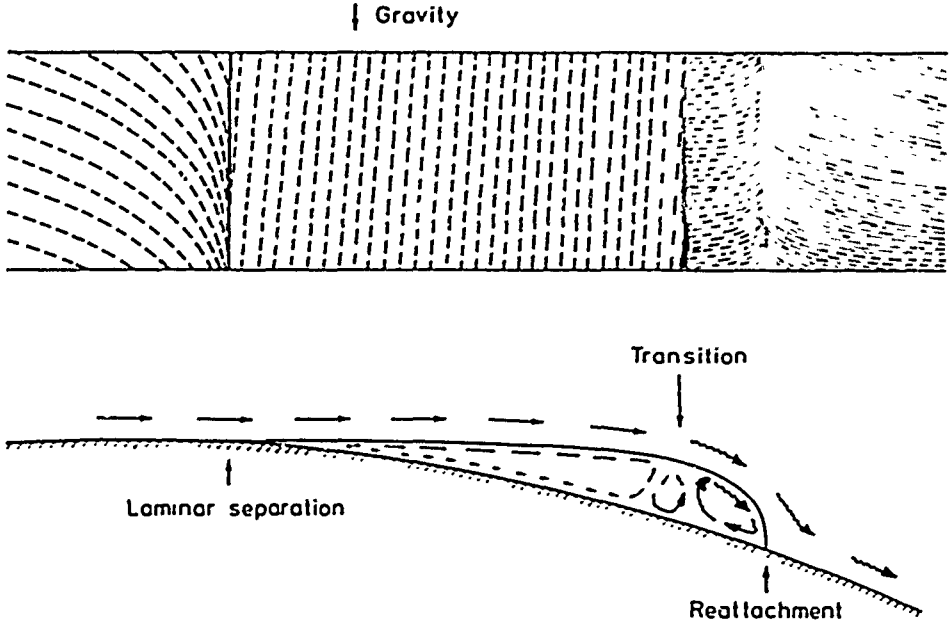

Fig. 2 Schematic view of assumed internal flow in a laminar separation bubble and oil flow pattern on a model vertically installed in the wind tunnel

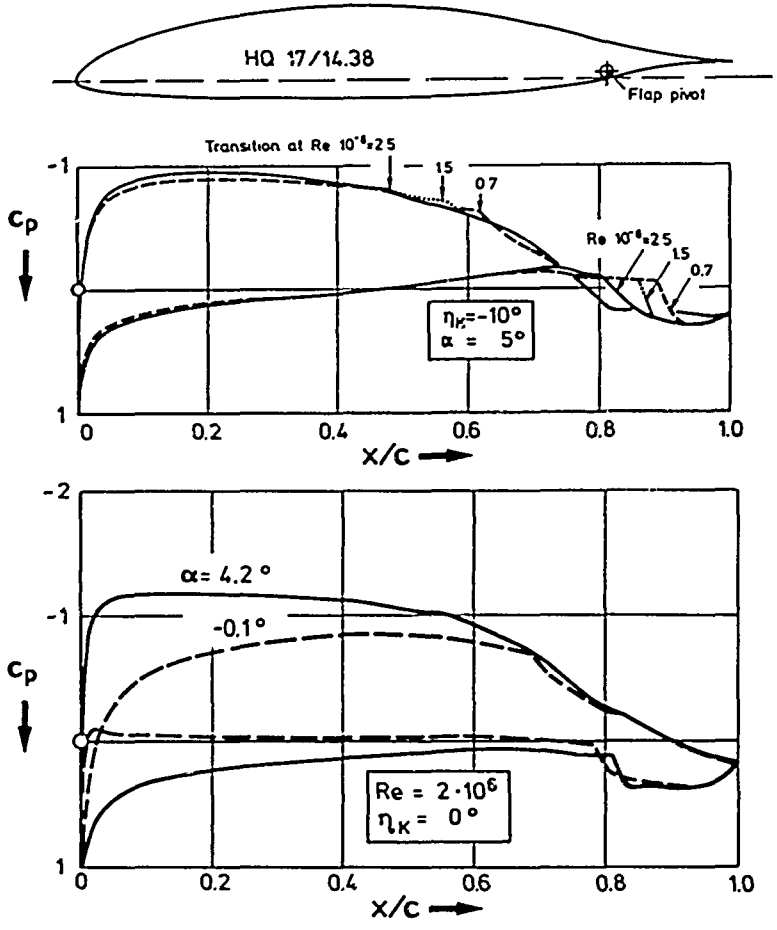

Fig. 3 Size and position of the laminar separation bubble as a function of Reynolds number and angle of attack of airfoil section DFVLR HQ 17/14.38 (Measurements TH Delft)

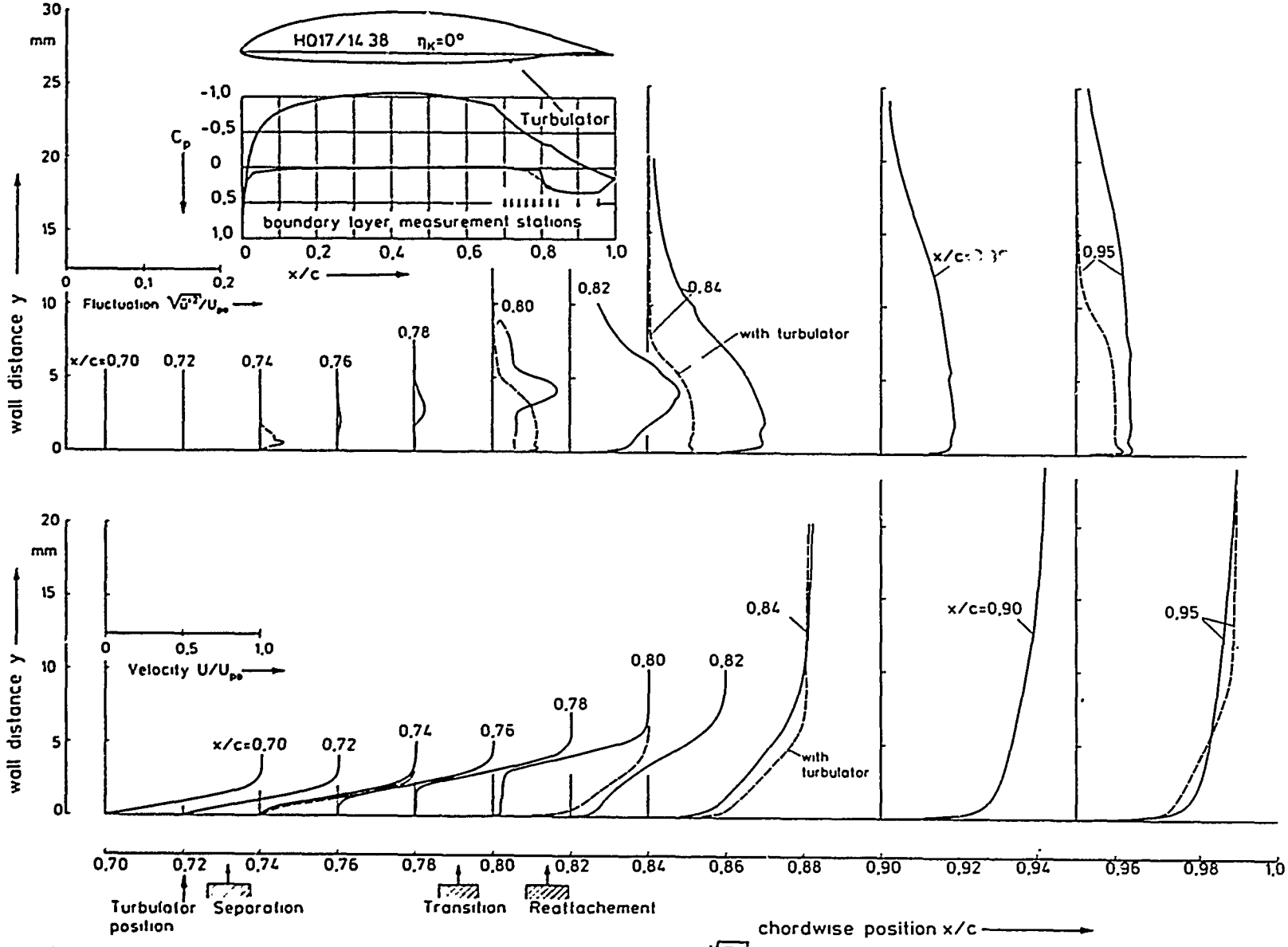

Figure 4 Boundary layer velocity U/U_{po} and fluctuation $\sqrt{\bar{u}^2}/U_{po}$ profiles for lower surface of airfoil HQ 17/14.38 with and without laminar separation bubble, Re = $2 \cdot 10^6$ (Measurements TH Delft)

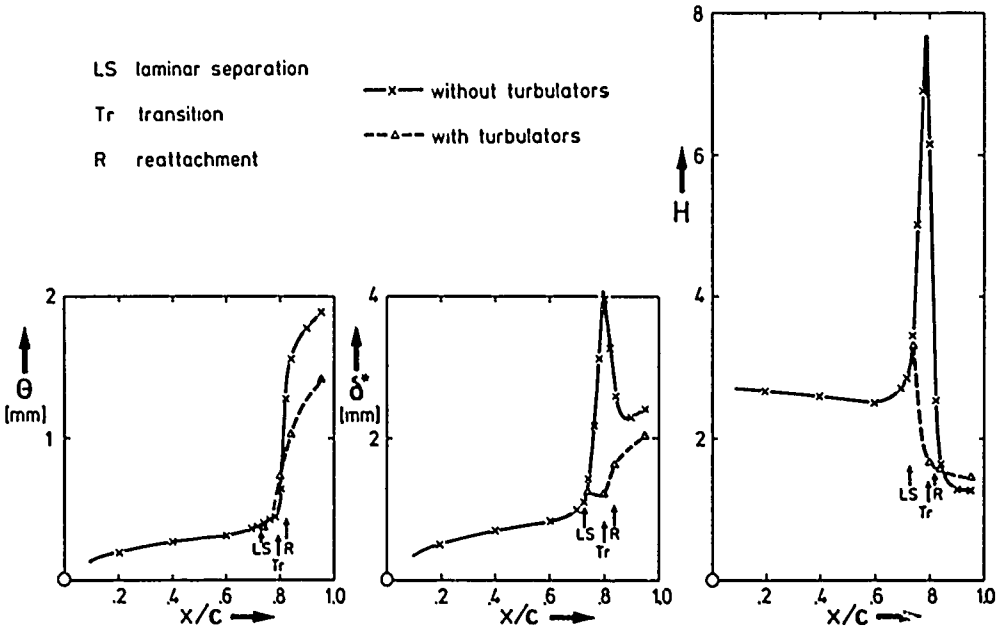

Fig. 5 Development of boundary layer parameters calculated from the velocity profiles in figure 4 (Measurements TH Delft)

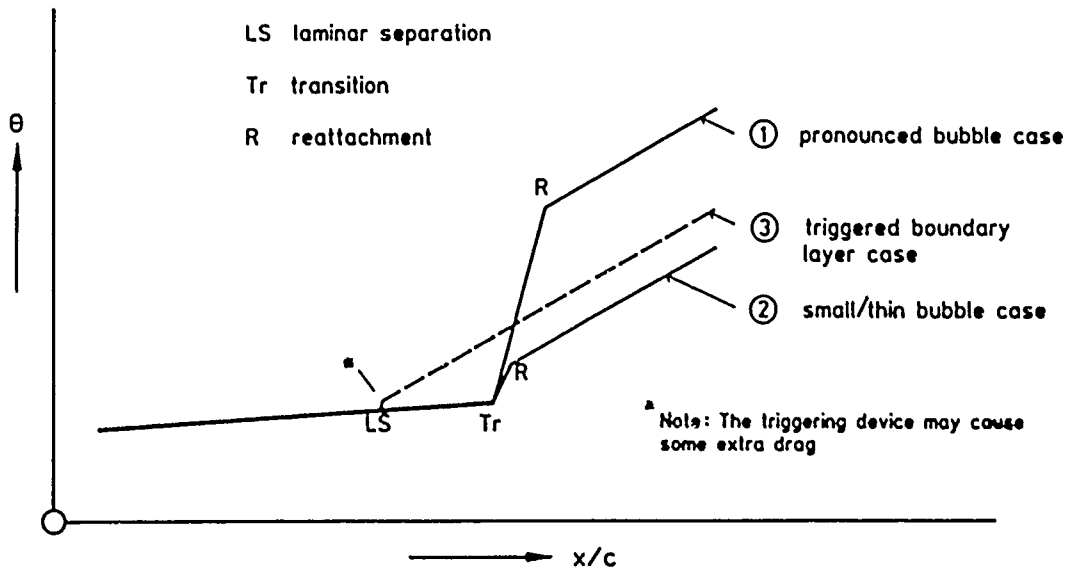

Fig. 6 Schematic sketch of the development of the momentum loss thickness in three typical cases

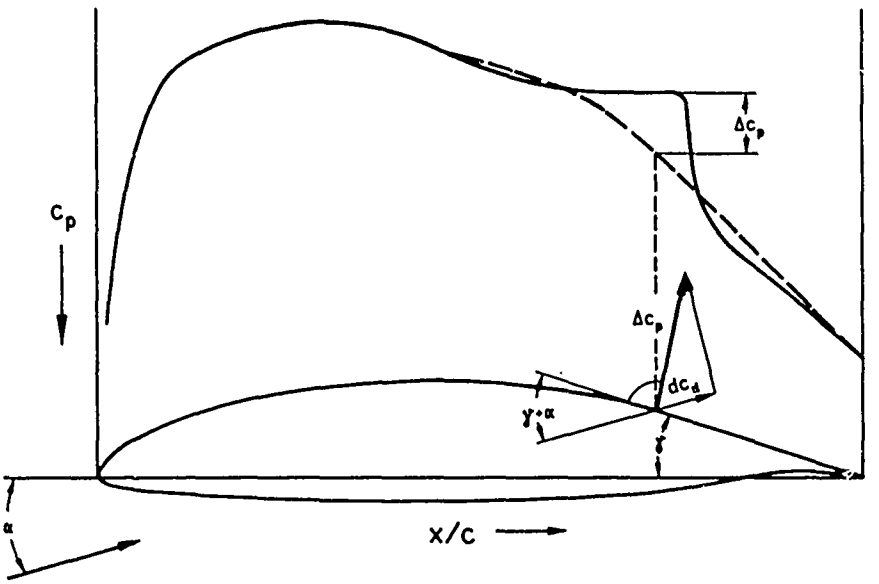

Fig. 7 Schematical representation of the additional pressures Δc_p acting on an airfoil as a result of a laminar separation bubble

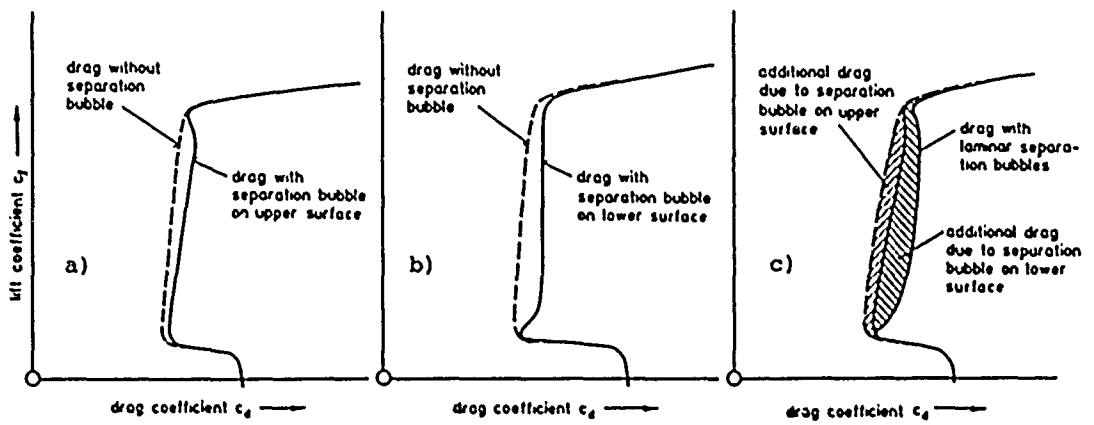

Fig. 8 Assumed development of additional drag caused by laminar separation bubbles on upper and lower surface of an airfoil section

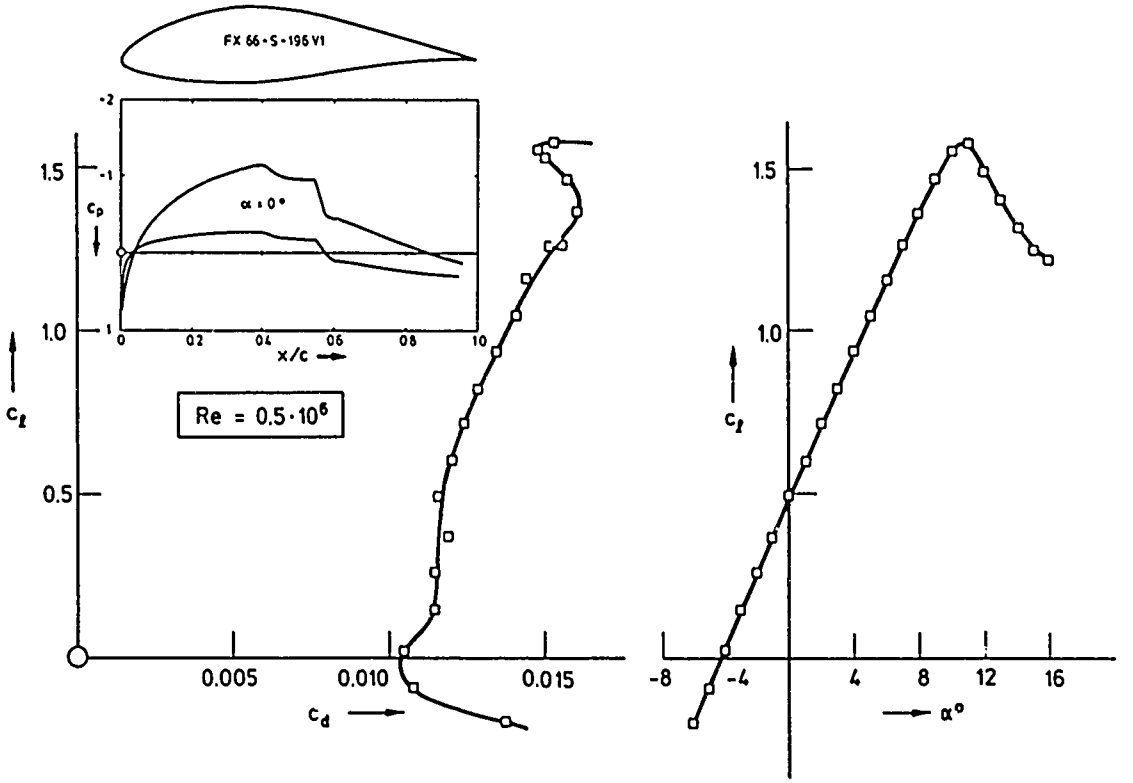

Fig. 9 Characteristics of the FX 66-S-196 V1 Wortmann airfoil section at Re = $0.5 \cdot 10^6$ (Measurements TH Delft [3])

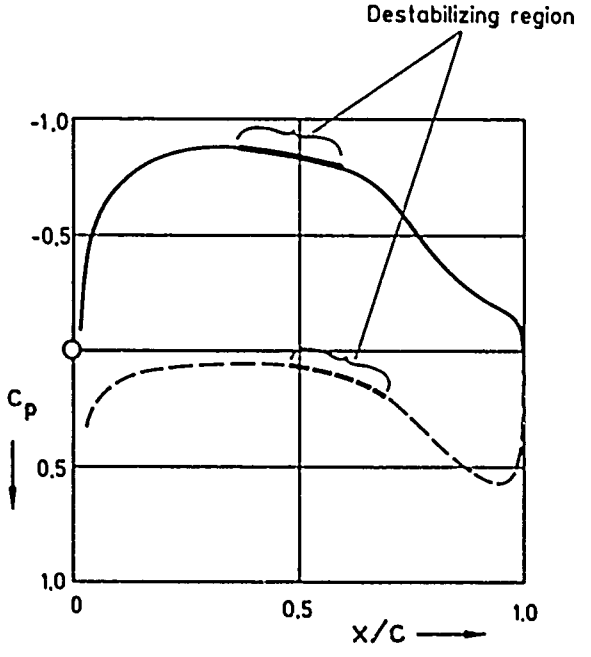

Fig. 10 Airfoil section with destabilizing regions (potential flow calculation of Wortmann airfoil section FX 62-K-131)

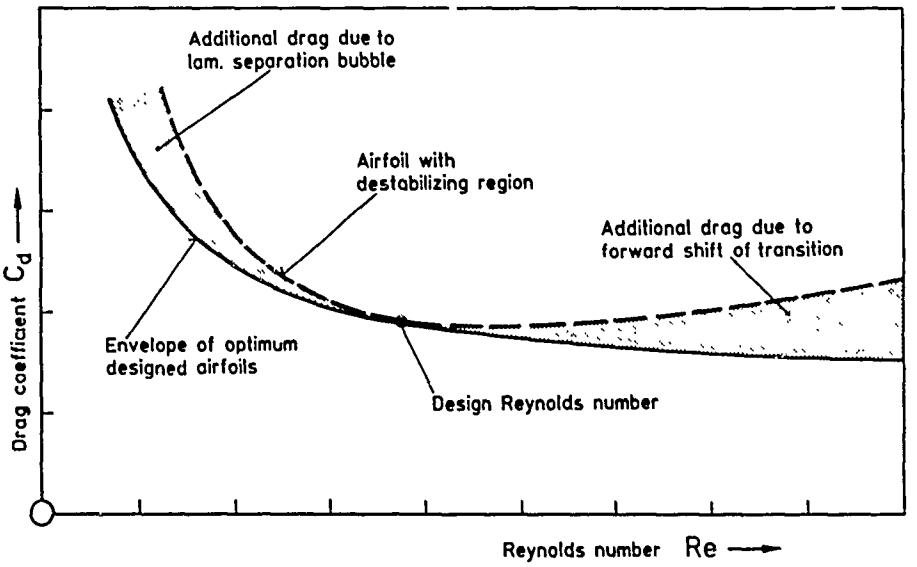

Fig. 11 Diagrammatic representation of the drag curve plotted against Reynolds number for airfoil sections with destabilizing regions

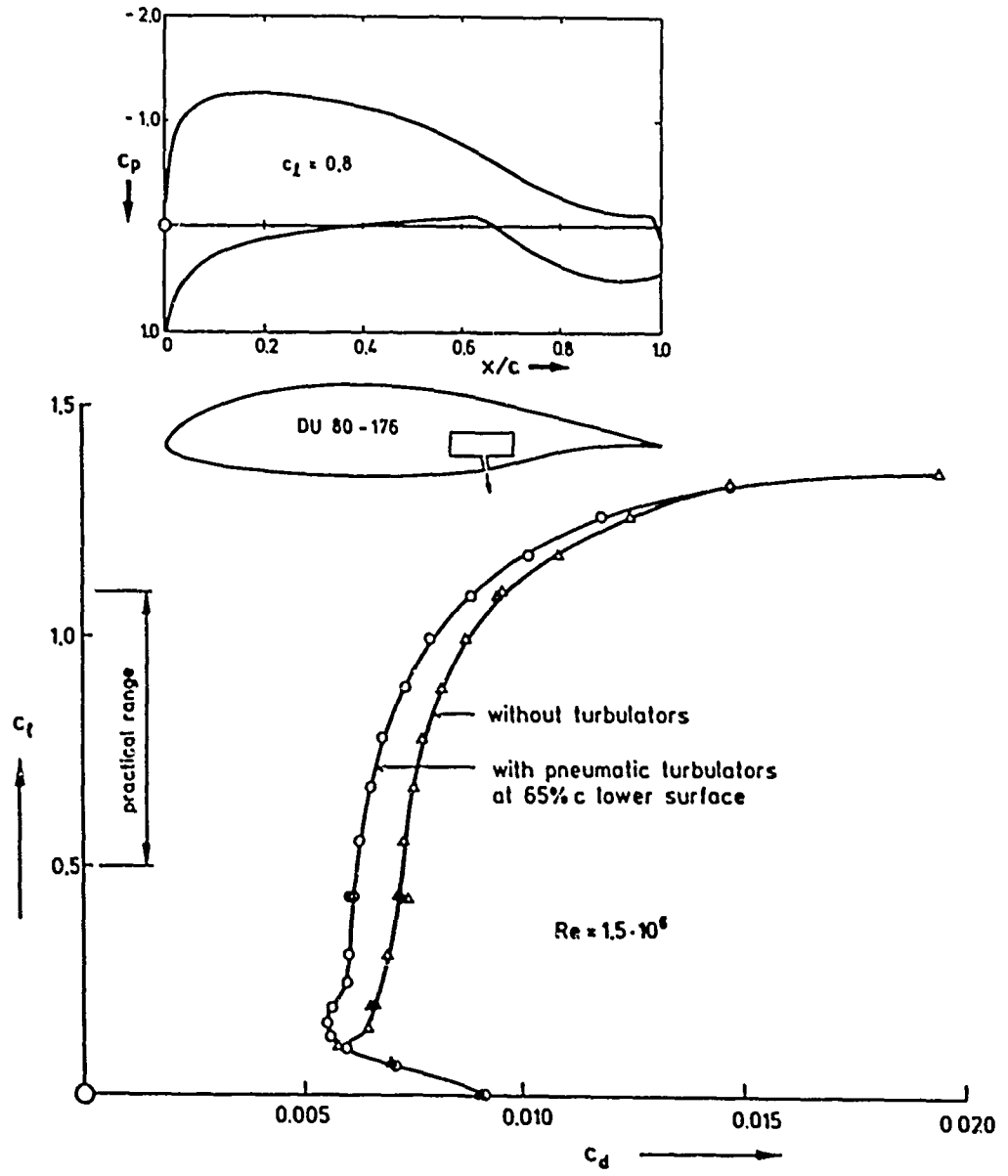

Fig. 12 Drag polar and potential flow pressure distribution of Delft University airfoil DU 80-176

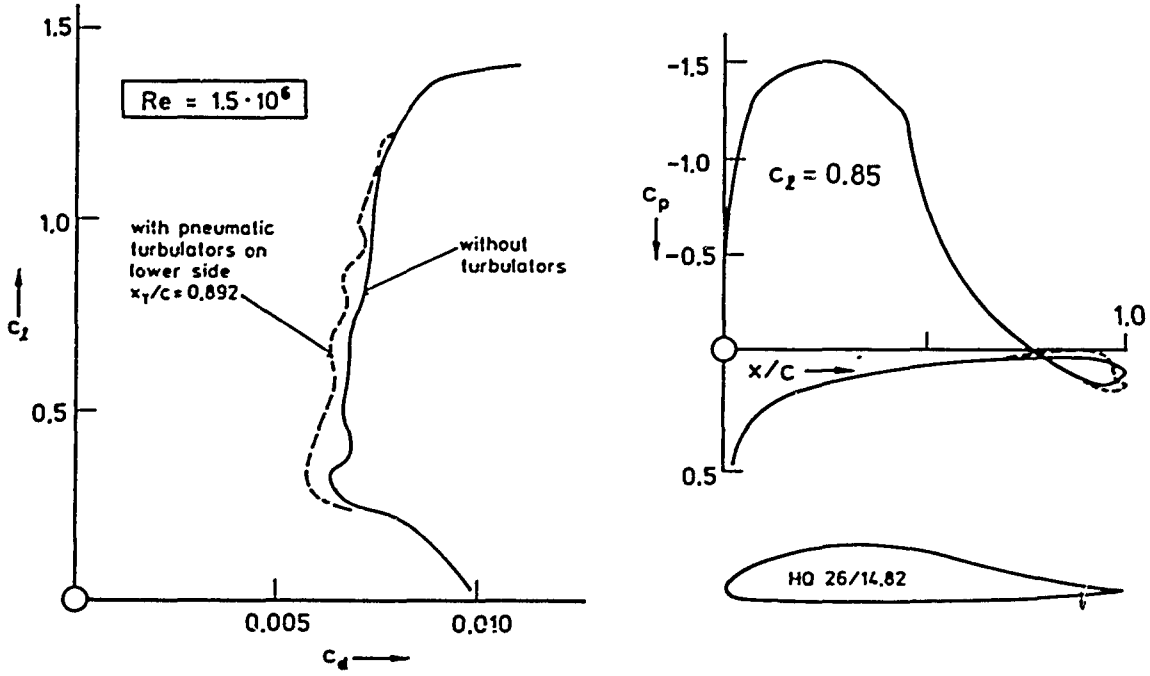

Fig. 13 Drag polar and measured pressure distribution of airfoil DFVLR-HQ 26/14.82 (Free flight measurements DFVLR Braunschweig)

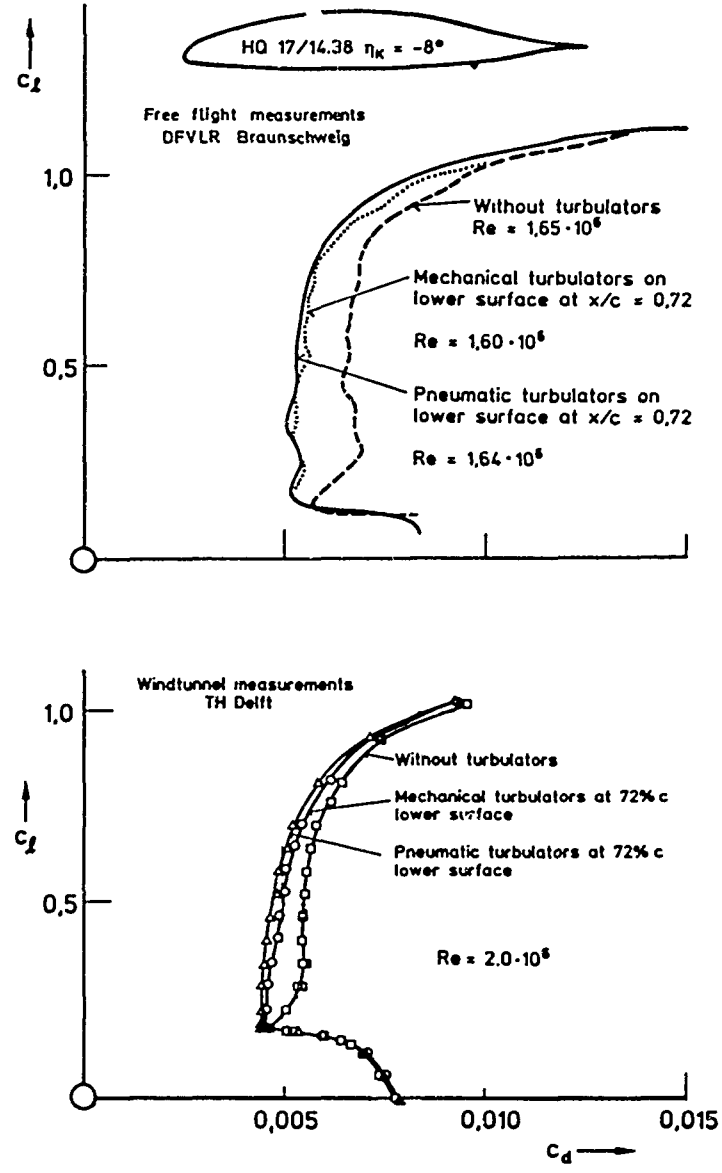

Fig. 14 Results of free flight and windtunnel measurements on HQ 17/14.38 with and without turbulators

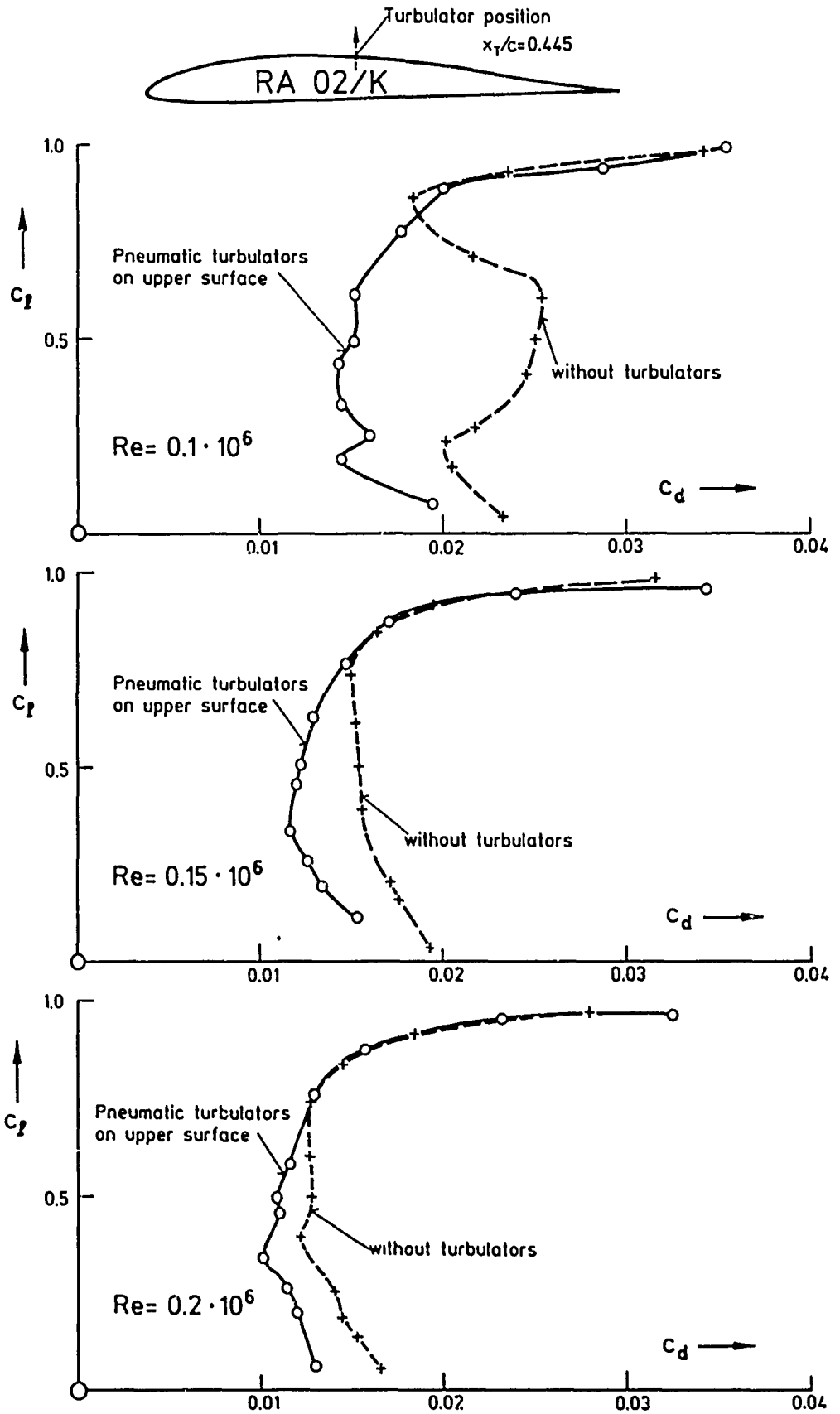

Fig. 15 Drag polars of the airfoil DFVLR RA 02/K with and without pneumatic turbulators (Measured in small cascade windtunnel DFVLR Braunschweig [14])

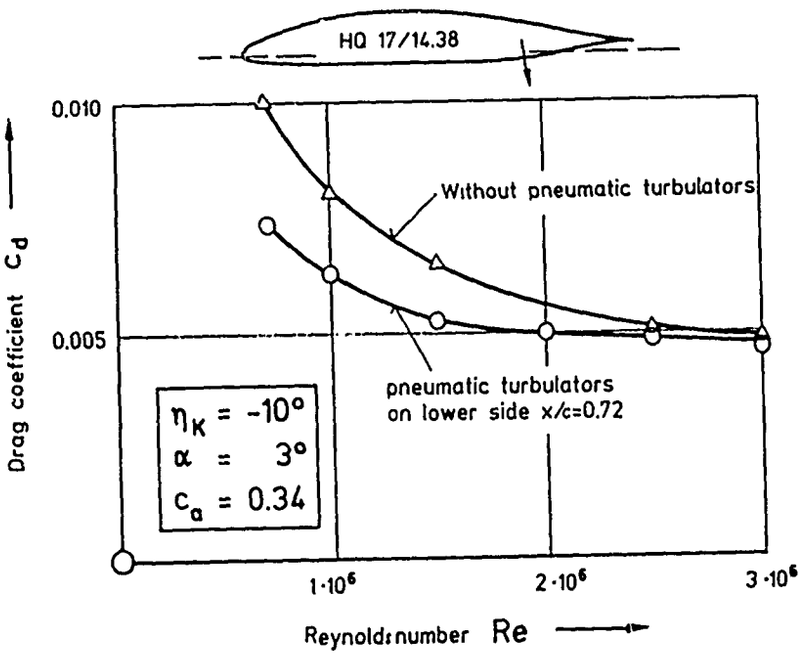

Fig. 16 Drag reduction by turbulators depending on Reynolds number (Measurements TH Delft)

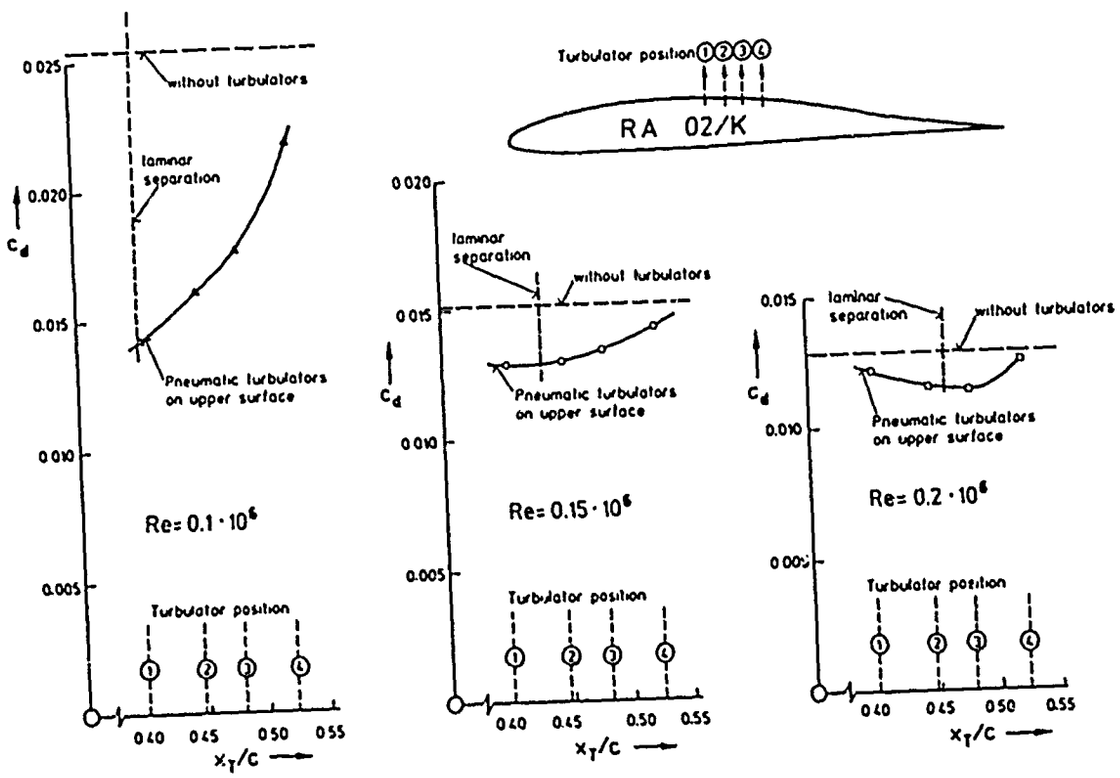

Fig. 17 Drag reduction depending on pneumatic turbulator position of airfoil RA 02/K at c_ℓ = 0.6 (Measured DFVLR Braunschweig [14])

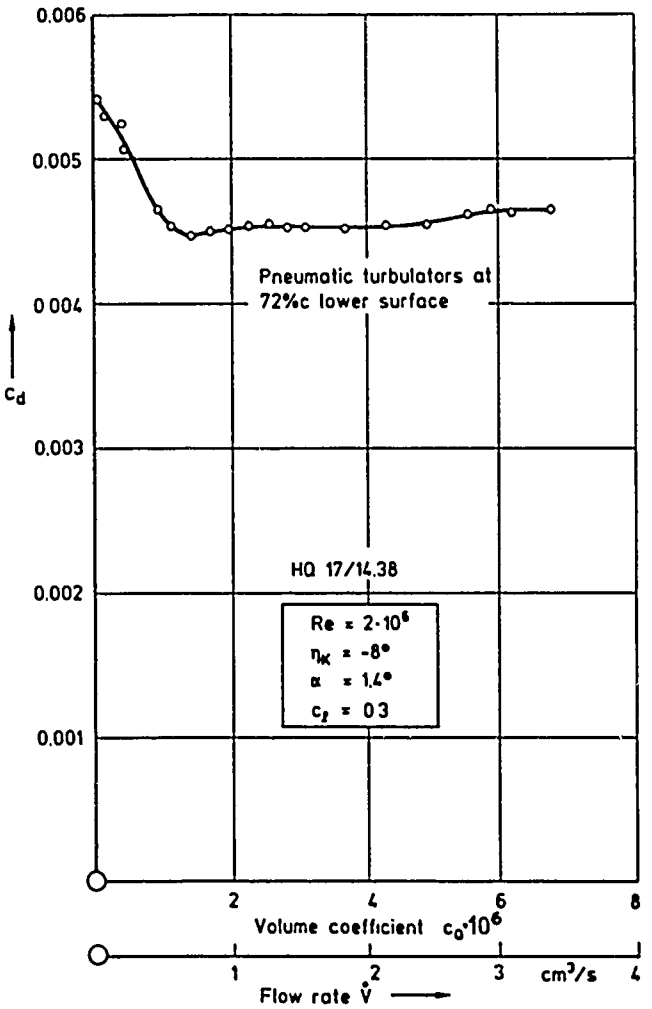

Fig. 18 The drag of airfoil HQ 17/14.38 with various air jet coefficients c_Q and volume flow $\dot{V}$ per hole (Measurements TH Delft)

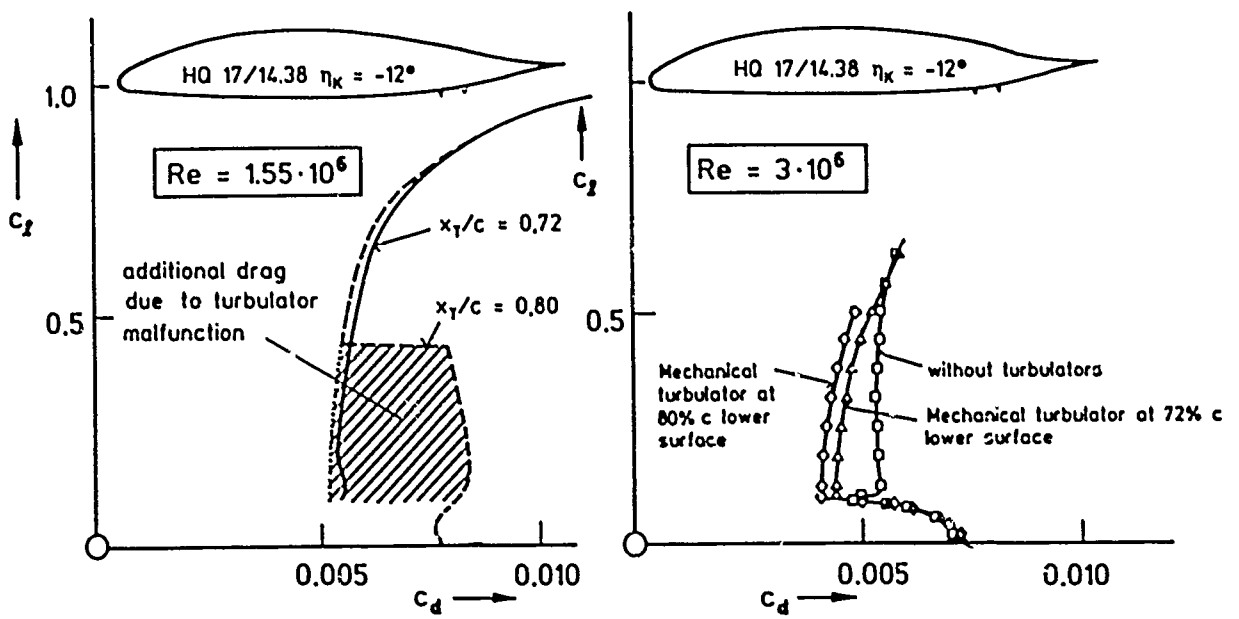

Fig. 19 Results of free flight and windtunnel measurements on airfoil HQ 17/14.38 with and without mechanical turbulators
(Re = 1.55 · 10^6: Free flight measurements DFVLR Braunschweig
Re = 3.0 · 10^6: Windtunnel measurements TH Delft)